Chem Soc Rev

TUTORIAL REVIEW

View Article Online
View Journal | View Issue

Cite this: *Chem. Soc. Rev.*, 2018, **47**, 5588

Omnipotent phosphorene: a next-generation, two-dimensional nanoplatform for multidisciplinary biomedical applications

Meng Qiu,†[ab] Wen Xiu Ren,†[a] Taeho Jeong,†[a] Miae Won,[a] Geun Young Park,[a] David Kipkemoi Sang,[b] Li-Ping Liu,[c] Han Zhang *[b] and Jong Seung Kim *[a]

Received 30th April 2018

DOI: 10.1039/c8cs00342d

rsc.li/chem-soc-rev

Phosphorene, also known as single- or few-layer black phosphorus (FLBP), is a new member of the two-dimensional (2D) material family and has attracted significant attention in recent years for applications in optoelectronics, energy storage and biomedicine due to its unique physicochemical properties and excellent biocompatibility. FLBP is regarded as a potential biological imaging agent for cancer diagnosis due to its intrinsic fluorescence (FL) and photoacoustic (PA) properties and negligible cytotoxicity. FLBP-based photothermal and photodynamic therapies have emerged with excellent anti-tumour therapeutic efficacies due to their unique physical properties, such as near-infrared (NIR) optical absorbance, large extinction coefficients, biodegradability and reactive oxygen species (ROS) or heat generation upon light irradiation. Furthermore, FLBP is a promising drug delivery platform because of its high drug-loading capacity due to its puckered layer structure with an ultralarge surface area, and FLBP is size-controllable with facile surface chemical modification. Because of the marked advantages of FLBP nanomaterials in biomedical applications, an overview of the latest progress and paradigms of FLBP-based nanoplatforms for multidisciplinary biomedical applications is presented in this tutorial review.

Key learning points

(1) Overview of the general significance of FLBP in biomedical science.
(2) Summary of the latest development of FLBP, ranging from structures, preparations, and photophysical and chemical properties to biocompatibility.
(3) Introduction to the designing strategies of FLBP-based nanoplatforms for biomedical applications.
(4) Discussion of the diverse biological applications of FLBP-based nanoplatforms such as various bioimaging techniques, phototherapy, therapeutic agent delivery, *etc.*
(5) Perspectives and potential future directions for FLBP-based nanoplatforms for biomedical applications.

1. Introduction

Novoselov and Geim[1] discovered graphene in 2004, and two-dimensional (2D) nanomaterials have been noted to play essential roles in various fields of science and technology due to their unique physical and chemical properties.[2] In contrast to traditional bulky materials, 2D nanomaterials provide large specific surface areas for cargo loading and functional modifications, and their single-atomic layers exhibit excellent photophysical and photochemical properties, which are favourable for developing novel, multifunctional nanoplatforms for combination strategies. In particular, in the biomedical field, 2D nanomaterials have potential for new applications in optical imaging, biosensing, phototherapy, targeted delivery and other fields. However, practical applications of 2D nanomaterials are limited by their intrinsic shortcomings. Despite possessing higher carrier mobilities, the zero bandgap of graphene and the limited bandgaps of transition metal carbides, nitrides and carbonitrides (MXenes) hinder their applications in optical sensing, bioimaging, and field effect transistors (FETs). Though transition metal dichalcogenides (TMDs) have a finite bandgap, their low carrier mobility prevents their applications in many

[a] *Department of Chemistry, Korea University, Seoul 02841, Korea. E-mail: jongskim@korea.ac.kr*
[b] *Shenzhen Engineering Laboratory of Phosphorene and Optoelectronics and Key Laboratory of Optoelectronic Devices and Systems of Ministry of Education and Guangdong Province, Shenzhen University, Shenzhen 518060, P. R. China. E-mail: hzhang@szu.edu.cn*
[c] *Department of Hepatobiliary and Pancreatic Surgery, Shenzhen People's Hospital, The Second Clinical Medical College of Jinan University, Shenzhen 518060, P. R. China*
† These authors contributed equally to this work.

sensing fields. The 2D hexagonal boron nitride (h-BN) is a good proton conductor with a high electrical resistance, but its insulating properties limit its other applications. Therefore, an omnipotent nanomaterial with a well-balanced performance is in great demand.

Recently, as a new 2D material, single- or few-layer black phosphorus (FLBP) has attracted considerable attention for applications in optoelectronics, energy storage and biomedicine. FLBP is reported to be superior to the abovementioned 2D materials due to its exceptional properties.[4–6] FLBP has a direct and layer-dependent bandgap, which can be tuned from 0.3 to 2 eV by decreasing its thickness from bulk to monolayer. The appealing tunable bandgap of FLBP holds great promise in bridging the space between zero-gap graphene, limited bandgap MXenes, large-gap TMDs and insulator h-BN. Therefore, the strong interactions between FLBP and electromagnetic waves can be easily manipulated in a layer-dependent manner in the ultraviolet (UV) and near-infrared (NIR) regions, endowing FLBP with a large extinction coefficient and photoredox capability and providing FLBP with excellent optical properties compared to those of other 2D materials. In addition, FLBP possesses a moderate ON/OFF ratio (10^4–10^5) while preserving a sufficiently large carrier mobility ($\sim$1000 cm^2 V^{-1} s^{-1}). Based on its intriguing properties, FLBP is suitable for many applications such as FET sensing-based gas and biodetection as well as bioimaging. Furthermore, the puckered layer structure of FLBP is held together by van der Waals forces and provides an ultralarge surface area where many drugs, bioactive molecules, fluorescent molecules and metal atoms can be loaded *via* nondestructive non-covalent bonds, which maintain the bioactivity of the loaded agents and allow a number of biological applications, *e.g.*, targeted drug delivery, biomolecule detection, cell imaging, and cancer therapy.[7–14] FLBP is a versatile platform for constructing a range of multifunctional nanostructures due to its mechanical flexibility. Most importantly, FLBP has negligible cytotoxicity and excellent biodegradability in the body compared to those of other common 2D nanomaterials, indicating that FLBP could be an omnipotent nanoplatform for multidisciplinary biomedical applications.[15]

Recent years have witnessed many breakthroughs in FLBP fundamental research and applications.[16–19] Because of the rising interest in FLBP, since 2014, a number of research papers related to FLBP have been published in the fields of optoelectronics and energy storage.[6,20,21] In addition, in biomedical fields, several FLBP-based nanoplatforms for anticancer treatments have been reported over the past three years.[7,9,15,22–27] However, comprehensive reviews on FLBP-based nanomaterials and their biomedical applications have rarely been published. In this review, after a brief introduction of the basic physical and chemical properties of FLBP, we mainly focus on FLBP-based nanoplatform applications in biomedical fields, including bioimaging techniques, photothermal therapy (PTT),

Front line: Dr Meng Qiu, Prof. Jong Seung Kim, and Dr Wen Xiu Ren; Back line: Dr Miae Won, Taeho Jeong, and Geun Young Park (from left to right)

Meng Qiu was born in Qingdao, China, in 1983. He received his PhD from the Institute of Chemistry, Chinese Academy of Sciences, in 2013. He joined Prof. Han Zhang's lab in Shenzhen University, and then joined Prof. Jong Seung Kim in Korea University as a research professor. His research interests focus on two-dimensional material based theranostic nanoplatforms for biomedical applications.

Prof. Jong Seung Kim received his PhD from the Department of Chemistry and Biochemistry at Texas Tech University in 1993 and continued his research in the University of Houston as a postdoc. He is now a professor in the Department of Chemistry at Korea University in Seoul. To date, he has published over 400 scientific publications and 70 patents. He is currently a member of the Korea Academy of Science and Technology.

Wen Xiu Ren was born in Changchun, China, in 1981. In 2009, he obtained his PhD from Kyungpook National University and continues his research under the supervision of Prof. Jong Seung Kim as a research professor in Korea University. His research interests include fluorescent chemosensors and the development of new anticancer theranostic systems.

Miae Won was born in Seoul, Korea, in 1981. She received her PhD from the Department of Pharmacy at CHA University in 2017. In the same year she joined Prof. Jong Seung Kim's group in Korea University as a research professor. Her current research interests focus on the development and validation of novel bio-probes for sensing and imaging of cancer, and chronic diseases using various advanced molecular and genetic methods.

Taeho Jeong was born in Daegu, Korea, in 1992. He is pursuing his master's degree under the guidance of Prof. Jong Seung Kim in the Department of Chemistry at Korea University. His research interests include the development of novel biomarkers and drug delivery frameworks for cancer therapeutics.

Geun Young Park was born in Masan, Korea, in 1993 and earned her bachelor's degree from the Department of Chemistry from Kyung Hee University in 2017. She has worked toward her master's course under the guidance of Prof. Jong Seung Kim. Her current research interests are focused on cancer targeted drug delivery systems and their imaging.

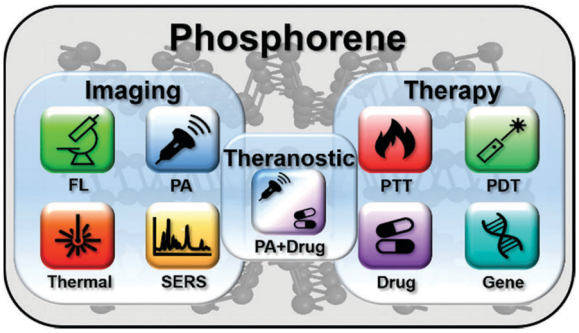

Fig. 1 The multidisciplinary biomedical applications of phosphorene, including diagnostic imaging, phototherapy, therapeutic agent delivery and theranostics.

photodynamic therapy (PDT), drug delivery and combination strategies, as illustrated in Fig. 1.

2. Black phosphorus discovery and few-layer black phosphorus preparation

2.1. Black phosphorus discovery

Black phosphorus (BP) was discovered approximately 100 years ago. In 1914, Bridgman[28] found BP during the process of converting white phosphorus to red phosphorus by subjecting white phosphorus to high pressure and temperature. Twenty years later, in 1935, Hultgren *et al.*[29] determined the crystal structure of BP by X-ray diffraction and demonstrated that BP has an orthorhombic structure and is a thermodynamically stable phosphorus allotrope. The physical, electronic and structural properties of BP are very much like those of graphite – *i.e.*, both are black and flaky conductors with layered sheets of linked atoms. Later, red phosphorus was also transformed into crystalline BP.[30] However, compared with the other two allotropes (white and red phosphorus), BP has not attracted much attention over the past century because of its poor preparation conditions and limited applications.

Since the unique optoelectronic properties of FLBP were revealed in 2014,[31] FLBP has gained considerable interest in the materials research community. Unlike graphene, the sp^3 hybridization of phosphorus atoms within the phosphorene structure forms a triangular pyramid structure, which forms a bilayer configuration along the zigzag direction and a puckered architecture along the armchair direction.

FLBP exhibits many excellent properties owing to its unique structure. FLBP is the thinnest direct bandgap semiconductor with a layer-dependent bandgap that can be tuned from 0.3 to 2.0 eV by downsizing the bulk to monolayer units. Furthermore, the FLBP within the planes of the layers has unique optical, mechanical, and thermoelectric properties, electrical conductance and Poisson's ratio, causing it to behave in a highly anisotropic manner and exhibit significant potential for applications in thin-film electronics and optoelectronics.[32]

More importantly, the biodegradability of FLBP is a paramount advantage in its biomedical applications. Although BP bulk crystals are stable for several months, FLBP is slightly unstable in the presence of moisture under light irradiation in air. FLBP less than 10 nm thick without proper protection degrades in days, and single- and double-layer BP degrade within hours (Fig. 2A).[43] In 2016, Zhou *et al.*[44] proposed an ambient FLBP degradation mechanism using *ab initio* calculations and suggested a three-step FLBP ambient degradation mechanism. First, superoxide anions (O_2^-) are generated *via* a charge transfer reaction on the FLBP surface under ambient light. A thinner FLBP surface with a smaller barrier produces more O_2^- due to the thickness-dependent bandgaps. Then, the

David Kipkemoi Sang, Prof. Han Zhang, Dr Li-Ping Liu (from left to right)

David Kipkemoi Sang was born in Narok County, Kenya, in 1983. He obtained his master's degree from the Beijing University of Chemical Technology in Chemical Engineering and Technology in 2016. He is currently pursuing his PhD degree under the guidance of Prof. Han Zhang at Shenzhen University in Optoelectronic Engineering. His research interests focus on the study of novel two-dimensional systems using theoretical modeling.

Prof. Han Zhang was born in Wuhan, China, in 1984. He received his BS degree from Wuhan University in 2006 and PhD from Nanyang Technological University in 2010. He is currently a director of the Shenzhen Key Laboratory of 2D Materials and Devices, and the Shenzhen Engineering Laboratory of Phosphorene and Optoelectronics, Shenzhen University. To date, he has published over 203 scientific publications and 38 patents. His current research focus is the ultrafast and nonlinear photonics of two dimensional materials.

Li-Ping Liu was born in Hunan Province, China, in 1982. He received his PhD from the Department of Surgery at the Chinese University of Hong Kong. He joined the Department of Hepatobiliary and Pancreas Surgery, the Second Clinical Medical College of Jinan University, in 2012 as an associate consultant doctor. His current research focus is biological nanomaterials and tumors. His research records include 30 scientific publications.

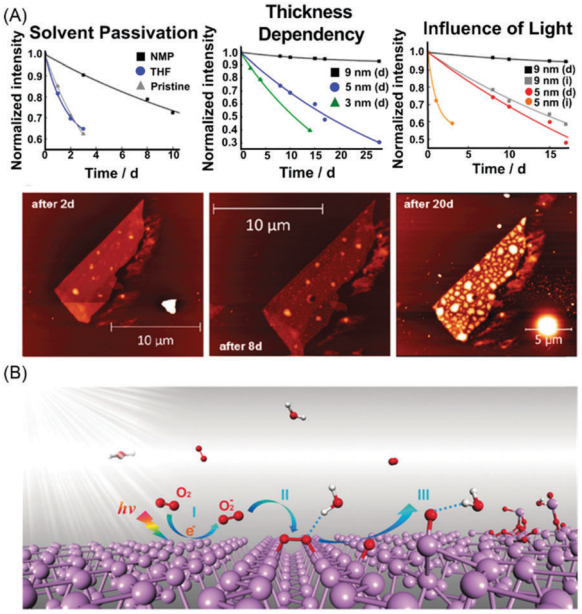

Fig. 2 (A) Influence of solvent passivation, thickness and visible-light illumination on FLBP. (B) The proposed degradation mechanism of FLBP under ambient conditions using *ab initio* calculations. (A) is reproduced with permission from ref. 4, Copyright 2014, IOP Publishing. (B) is reproduced with permission from ref. 44, Copyright 2016, John Wiley and Sons.

dissociated O_2^- species react with phosphorus on the FLBP surface to produce two P–O bonds. Finally, water molecules interact with the bonded oxygen through hydrogen-bond interactions to remove the phosphorus clusters and break the top phosphorene layer (Fig. 2B). This study provided a precise FLBP biodegradability degradation mechanism in which the roles of light, oxygen, and moisture were clearly demonstrated. Moreover, FLBP tends to react with oxygen *in vivo* to produce nontoxic products, such as phosphite ions, phosphate ions, and other P_xO_y species, which do not cause environmental problems.[15] Compared to other 2D materials such as graphene, TMDs and MXenes, which are non-biodegradable and can be excreted from the body only by liver detoxification and kidney (renal) micturition, the negligible toxicity and excellent biodegradability of FLBP are advantages for various biological applications.

Since FLBP has many advantageous properties, strategies to develop FLBP are currently being researched.

2.2. Few-layer black phosphorus preparation

The production of FLBP has been achieved in many research studies over the past three years, and these production methods can be categorized as top-down (*e.g.*, mechanical cleavage and liquid-phase exfoliation) and bottom-up (*e.g.*, chemical vapor deposition (CVD) and wet-chemistry) methods, which are depicted in Fig. 3.

FLBP can be mechanically and easily exfoliated because of its weak van der Waals interlayer interactions. Like graphene, the traditional sticky-tape method and subsequent plasma-thinning process have been successful in exfoliating FLBP to generate

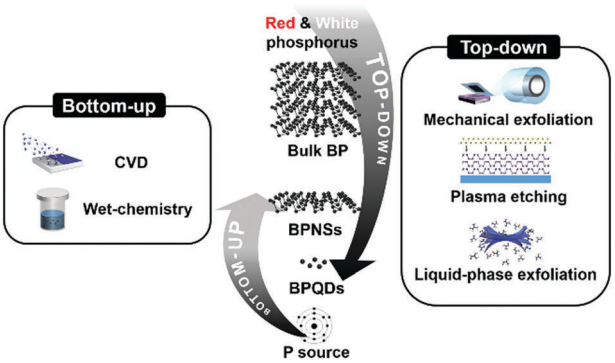

Fig. 3 Schematic illustration of FLBP preparation methods. Reproduced with permission from ref. 2, Copyright 2012, Nature Publishing Group, ref. 4, Copyright 2014, American Chemical Society, ref. 31, Copyright 2014, Nature Publishing Group, respectively, ref. 38 and 39, Copyright 2016, John Wiley and Sons.

uniform FLBP surfaces in a controllable manner.[2,31] However, for practical applications, those techniques have shortcomings such as low yields and a lack of morphology control.

Fortunately, these problems were resolved by the liquid-phase exfoliation method, which is a comparatively simple and inexpensive process. This process is advantageous for the scale-up production and bio-applications of FLBP. Brent *et al.* reported the first demonstration of liquid-phase exfoliation. They used sonication and NMP as an organic solvent.[16] Other organic solvents such as DMSO, DMF, IPA, and ethanol were also used, and their performances for the efficient preparation of FLBP were compared. Polar aprotic solvents are suitable for the preparation of FLBP.[17,18] In addition, many other methods, *e.g.*, ionic liquid solvents to obtain high-concentration FLBP,[33] fast and manageable electrochemical ion intercalation for high-efficiency exfoliation,[34] industrially scalable high-shear exfoliation,[35] and microwave-assisted exfoliation, have been widely investigated. In those FLBP exfoliation processes, an aqueous solution was also used as a solvent to avoid residual organic solvents.[9] However, FLBP easily aggregates and rapidly degrades during the process because of its low stability and high activity in aqueous solutions. To circumvent this problem, Kang *et al.*[36] developed a new FLBP exfoliation method using a deoxygenated aqueous surfactant to produce good phosphorene dispersions in aqueous solvents that exhibit a remarkable opto-electronic performance.

In addition to the top-down method, the bottom-up method has also been demonstrated, as shown in Fig. 3. CVD can control the doping contents and thickness of FLBP to generate ultralarge FLBP with good crystallinity.[37,38] Furthermore, a wet-chemical solvothermal reaction method was employed to prepare FLBP from bulk red phosphorus precursors.[39]

FLBP surface modification for extensive biological applications is a major challenge because the FLBP surface does not have a reactive functional unit. The PEGylation method has been widely implemented to solve this issue. PEGylated FLBP is a multifunctional carrier that retains its physicochemical nature, and desired molecules can be easily linked to or

anchored on its surface. Thus, PEGylated FLBP can provide a diverse carrying ability, sufficient capacity, and targeting efficiency for accurate therapy and combination treatment. In some cases, FLBP is vulnerable to external interferences, including biomolecule adsorption and high ionic strengths, which cause self-aggregation and degradation. In 2016, Yu *et al.* introduced a sulfonic ester ligated titanium (TiL_4) to the FLBP surface by surface coordination to prepare FLBP@TiL_4 and determined that its stability was markedly enhanced in aqueous solutions.[40,41] Ryder *et al.*[42] covalently introduced aryl diazonium onto the FLBP surface and observed that aryl diazonium successfully suppressed the degradation process for several weeks under ambient conditions.

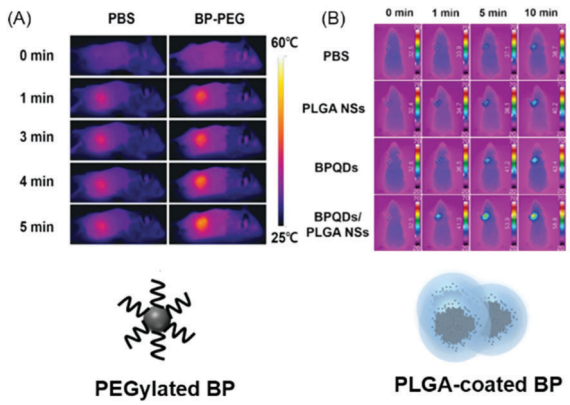

Fig. 4 NIR thermal imaging performance and structures of various FLBP nanosystems. (A) PEGylated FLBP and (B) PLGA-coated BPQDs. (A) is reproduced with permission from ref. 25, Copyright 2016, Elsevier. (B) is reproduced with permission from ref. 22, Copyright 2016, Nature Publishing Group.

3. Few-layer black phosphorus-based materials for biomedical applications

Recently, FLBP has been used to achieve a significant breakthrough in photoelectronic applications due to its unique electronic properties. The good photoelectronic properties of FLBP are also expected to be applicable to biomedical fields such as bioimaging, phototherapy and stimuli-responsive drug release. Furthermore, the low cytotoxicity, excellent biodegradability, good intrinsic aqueous dispersibility and relatively small size for the enhanced permeability and retention (EPR) effect of FLBP are ideal for biomedical applications.

3.1. Bioimaging

3.1.1. Fluorescence imaging. FLBP exhibits layer-dependent fluorescence (FL) spectra due to quantum size effects. Castellanos-Gomez *et al.*[3] reported that the photoluminescence of FLBP flakes strongly depends on their thickness. Thinner flakes have an intense peak at 775 nm, while thicker flakes are featureless. The weak photoluminescence from thick FLBP is due to its narrow bandgap outside the measurement window. Zhang *et al.*[4] also observed highly layer- and direction-dependent photoluminescence in FLBP. The FL intensity exponentially increases as the layer thickness decreases from five to two layers. Kang *et al.*[36] fabricated FLBP to show a high-exfoliation efficiency and observed its layer-dependent FL.

In 2016, Lee *et al.*[26] first investigated BP nanodots for biological imaging applications. They prepared bright fluorescent BP nanodots by a liquid-phase exfoliation method and found excitation wavelength-dependent FL (green and blue FL under 488 and 358 nm, respectively). Compared with other nanodots, BP nanodots exhibit negligible cytotoxicity in organisms and exhibit excellent fluorescence properties for potential bioimaging.

3.1.2. Photothermal imaging. FLBP has a high extinction coefficient and photothermal conversion efficiency (PTCE) due to the strong interactions between the FLBP crystal structure and electromagnetic waves within a vast energy spectrum ranging from the UV, visible to NIR region.[5,6] Many essential bio-applications including photothermal and photoacoustic (PA) imaging are based on these remarkable optical absorbance properties of FLBP.

Sun *et al.*[25] prepared PEGylated FLBP by a simple mechanical milling technique. Photothermal images of mice bearing 4T1 tumours treated with PEGylated FLBP under 808 nm laser irradiation are presented in Fig. 4A. The temperature of the tumour region dramatically increased from 34 to 59 °C within 5 min, whereas the temperature increased only 6 °C in the absence of FLBP. Shao *et al.*[22] fabricated poly(lactic-*co*-glycolic acid) (PLGA)-coated BP quantum dots (BPQDs) to improve the stability of the photothermal agent and showed that the tumour temperature of the mice treated with BPQDs/PLGA nanospheres rapidly increased by 26.3 °C under NIR-laser irradiation within 10 min, and the maximum temperature reached 58.8 °C (Fig. 4B). More recently, Qiu *et al.*[12,50] fabricated FLBP hydrogels, namely BP@hydrogel, for localized drug delivery and NIR-light thermal imaging. The photothermal effects were monitored upon intratumour injection of BP@hydrogel. The temperature of the BP@hydrogel-treated tumour increased by over 13 °C but did not increase with the control PBS solution.

3.1.3. Photoacoustic imaging. PA imaging, a biophotonic diagnostic modality, is a promising and superior *in vivo* bioimaging approach compared with other traditional optical imaging techniques because of its high image contrast, sensitivity, and spatial resolution. Photothermal and PA effects are proportional to the absorption cross-section of incident light. Therefore, more efficient PA imaging can be obtained with a larger PTCE.

In 2016, Sun *et al.*[25] reported that PEGylated FLBP has good aqueous solubility and biocompatibility as a novel PA imaging agent for cancer diagnosis. After intravenous injection, the higher signal intensity observed from a tumour suggested that the FLBP mainly accumulates in the tumour rather than other organs such as the kidneys and liver. Nevertheless, FLBP is unstable under physiological conditions, resulting in self-degradation and subsequent attenuation of the PA signal intensity. To resolve these problems, in 2017, Sun *et al.*[23]

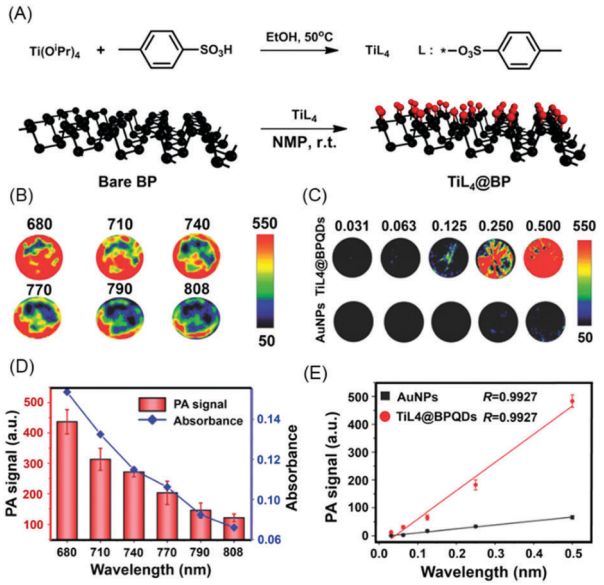

Fig. 5 (A) Synthesis and structural formula of TiL_4 and surface coordination of TiL_4 to BP. (B) PA images of TiL_4@BPQDs at different excitation wavelengths. (C) PA images of TiL_4@BPQDs and AuNRs with different optical densities at 680 nm. (D) PA signal and corresponding absorption intensities of TiL_4@BPQDs at different excitation wavelengths. (E) Corresponding signal intensities of TiL_4@BPQDs and AuNRs with different optical densities at 680 nm. Reproduced with permission from ref. 23, Copyright 2017, John Wiley and Sons.

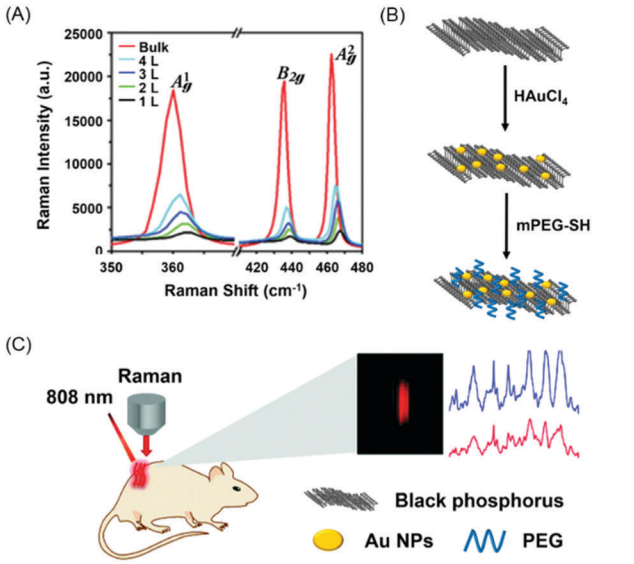

Fig. 6 (A) Raman spectra of bulk BP and FLBP. (B) Fabrication of BP–Au NSs and (C) the corresponding SERS-based bioimaging application. (A) is reproduced with permission from ref. 45, Copyright 2015, John Wiley and Sons. (B) and (C) are reproduced with permission from ref. 10, Copyright 2017, Royal Society of Chemistry.

reported TiL_4-coordinated BPQDs (Fig. 5A). Compared with the stability of bare BPQDs, TiL_4@BPQDs exhibited enhanced stability in water dispersions. Owing to their large NIR extinction coefficient, TiL_4@BPQDs display an excellent PA imaging performance in the NIR optical window (Fig. 5B and C). Laser irradiation at 680 nm induces a strong PA signal, and TiL_4 modification also creates a system with a better PA efficiency than Au nanorods (AuNRs) (Fig. 5D and E). Both *in vitro* and *in vivo* results confirmed excellent bioimaging performances for tracing tumours, demonstrating the enormous potential of TiL_4@BPQDs in biomedical applications.

3.1.4. Surface-enhanced Raman scattering imaging. Raman imaging with its ultrahigh specificity, relatively high penetration depth, and high-dimensional multiplexing potential is a viable alternative to fluorescence imaging of nanomaterials. By applying nanomaterial-enabled surface-enhanced Raman scattering (SERS) imaging, *in vivo* Raman imaging can be used for signal amplification in deep tissues. Though there are six Raman active modes, only three vibrational modes, one out-of-plane phonon mode (A_g^1 at 359 cm^{-1}) and two in-plane modes (B_{2g} and A_g^2 at 436 and 463 cm^{-1}, respectively), can be detected by Raman spectroscopy (Fig. 6A). Raman spectroscopy of FLBP is also layer-dependent. In 2015, Guo *et al.*[45] observed that Raman spectral peaks redshift and their intensities increase as the number of FLBP layers increases. They proposed that Raman spectral change is a simple and efficient method to measure the thickness of FLBP.

In 2017, Yang *et al.*[10] created gold nanoparticle (AuNP)-loaded FLBP nanosheets (BP–Au NSs) for effective SERS imaging (Fig. 6B). In addition to the enhanced PTT effect due to the BP–Au NSs, photothermal imaging can be monitored by a Raman technique that benefits from the high SERS activity of BP–Au NSs (Fig. 6C). The molecular fingerprint features of breast tumours before and after a PTT treatment were identified using a SERS analysis. The SERS analysis showed that upon incubation with BP–Au NSs under 808 nm NIR-laser irradiation the cell viability of the breast cancer 4T1 cells slightly decreased as the BP–Au NS concentration was increased up to 120 μg mL^{-1}. More than 85% of the 4T1 cells were alive upon incubation with BP–Au NSs at the highest concentration in the dark, indicating that the as-synthesized BP–Au NSs have an excellent biocompatibility and low cytotoxicity.

3.1.5. Biosensing. Detecting cancer markers in serum is one of the most common and important medical methods for early cancer detection and diagnosis. However, the cancer marker concentrations in serum are very low (pg mL^{-1} level) in the early stage of cancer. Therefore, a highly sensitive and selective detection method is needed to improve early cancer diagnosis.

In 2016, Yan *et al.*[46] demonstrated the first FLBP-based non-enzymatic hydrogen peroxide (H_2O_2) sensor by utilizing FLBP degradation under ambient conditions. The detection limit was measured to be 1×10^{-7} M. Kumar *et al.*[47] demonstrated the first aptamer-functionalized FLBP-based sensing platform for label-free detection of myoglobin (Mb), a cardiovascular disease biomarker (Fig. 7A). This aptamer-sensing platform showed a low detection limit (~0.524 pg mL^{-1}) and sensitivity (36 μA pg^{-1} mL cm^{-2}) for Mb with a dynamic response range of 1.0 pg mL^{-1} to 16 μg mL^{-1} in serum samples. Furthermore, Pumera *et al.*[13] reported a FLBP-based system for protein detection with a high selectivity. In a competitive immunoassay, FLBP was used as protein detection markers through the hydrogen

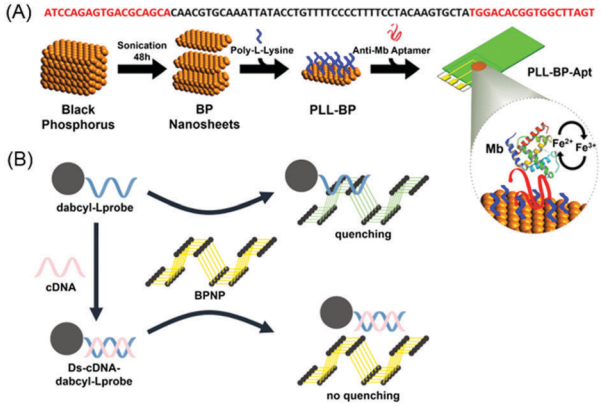

Fig. 7 (A) Schematic representation of the workflow for the liquid-phase exfoliation of FLBP and its surface modification for biointerface development on an electrode for Mb detection. (B) Schematic representation of the proposed DNA detection strategy based on FLBP as fluorophores. (A) is reproduced with permission from ref. 47, Copyright 2016, American Chemical Society. (B) is reproduced with permission from ref. 48, Copyright 2017, Royal Society of Chemistry.

evolution reaction due to the enhanced catalytic effect of the FLBP. FLBP was further employed as a fluorescence sensing platform for DNA detection for the first time (Fig. 7B). A wide linear detection range and low limits of detection and quantification were achieved by exploiting the differences in the affinities of the labelled single-stranded and double-stranded DNA oligonucleotides towards spontaneous self-assembly with FLBP.[48]

Gu *et al.*[49] fabricated a label-free sensing nanoplatform based on the interactions of BPQDs and 2-nitro-5-thiobenzoate anions (TNB) to evaluate the activity of acetylcholinesterase (AChE) with a high sensitivity (Fig. 8A). This nanoplatform was also used to evaluate the activity of AChE utilizing acetylthiocholine (Fig. 8B). In 2017, Peng *et al.*[14] developed a novel, simple, rapid and highly sensitive method for detecting cancer markers for the first time by utilizing the electronic properties of FLBP. They demonstrated that Au-decorated FLBP (BP–Au) has a high catalytic activity for

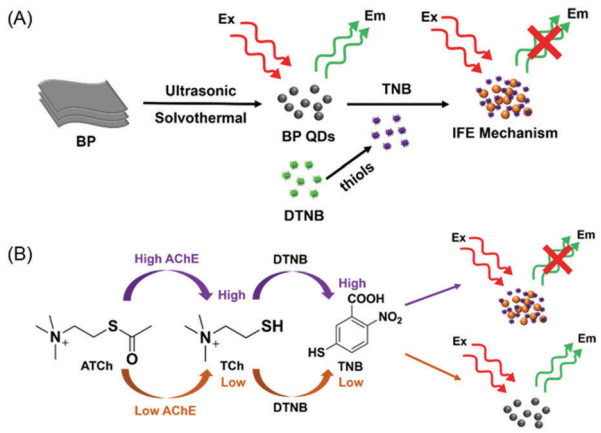

Fig. 8 (A) Schematic representation of the synthesis of BPQDs and (B) detection of thiols and the FL assay for AChE activity based on the inner filter effect mechanism. Reproduced with permission from ref. 49, Copyright 2017, Elsevier.

the reduction of yellow 4-nitrophenol to colourless 4-aminophenol (4-AP). Upon the addition of the carcinoembryonic antibody (anti-CEA), the catalytic activity of BP–Au can be reversibly 'switched off' due to the adsorption of the anti-CEA onto the Au surface, which inhibits the catalyst activity. However, the added carcinoembryonic antigen (CEA) binds to the anti-CEA to form an antigen–antibody complex in solution and shifts the equilibrium, causing the anti-CEA to desorb from the surface of BP–Au, which switches on the catalytic ability. Finally, a highly sensitive and selective colorimetric method for CEA detection was developed and used to detect CEA in clinical samples from colon and breast cancer patients.

3.2. Phototherapy

As an alternative to traditional cancer therapy, FLBP has been employed in phototherapy due to its many advantages such as minimal invasiveness and high therapeutic efficiency. In general, phototherapy is categorized as PTT and PDT. In PTT, the treatment is based on the heat energy generated from a PTT agent upon irradiation with light at a specific wavelength. In PDT, the treatment is based on the photochemical reaction of a photosensitizer (PS) triggered by light at a specific wavelength. In the process, many cytotoxic reactive oxygen species (ROS) are produced to kill targeted cancer cells in the light-exposed areas. Recently, many nanomaterials have been explored in cancer phototherapy with PDT and PTT, including graphene, TMDs, and MXenes. FLBP has also attracted attention as a potential PDT or PTT agent because of its impressive carrier mobility and tunable bandgap, which leads to its broad absorption across the UV, visible-light and NIR regions and ability to efficiently generate ROS or heat energy upon irradiation.

3.2.1. Photothermal therapy. Photothermal therapy (PTT) uses light-absorbing agents to induce hyperthermia under NIR light for tumour ablation, and PTT has been extensively explored and has received much attention in recent years. Compared with traditional cancer treatments, such as chemotherapy and radiotherapy, NIR-triggered PTT has fewer side effects due to its minimal dark toxicity and excellent therapeutic efficacy due to the easy manoeuvrability of light radiation. In the past decade, various graphene analogues, including TMDs and MXenes, have been developed as photothermal agents for tumour hyperthermia. However, their low PTCE and high cytotoxicity have hindered their biomedical applications.

FLBP nanomaterials display broad absorption over the entire visible-light region, which allows FLBP to exhibit photothermal activity that can be applied to PTT. In 2015, Sun *et al.*[27] synthesized BPQDs based on a controllable liquid-phase exfoliation technique using a probe with bath sonication (Fig. 9A). Upon PEG modification, the ultra-small BPQDs exhibited superior stability in PBS medium (Fig. 9B), an outstanding NIR photothermal performance with a large extinction coefficient (14.8 L g^{-1} cm^{-1} at 808 nm), a PTCE of 28.4% (Fig. 9C), comparatively high photostability (Fig. 9D), and negligible cytotoxicity (Fig. 9E). *In vitro* results showed that the NIR photoexcitation of BPQDs can cause significant cell death of both C6 and MCF7 cancer cells, which suggested the

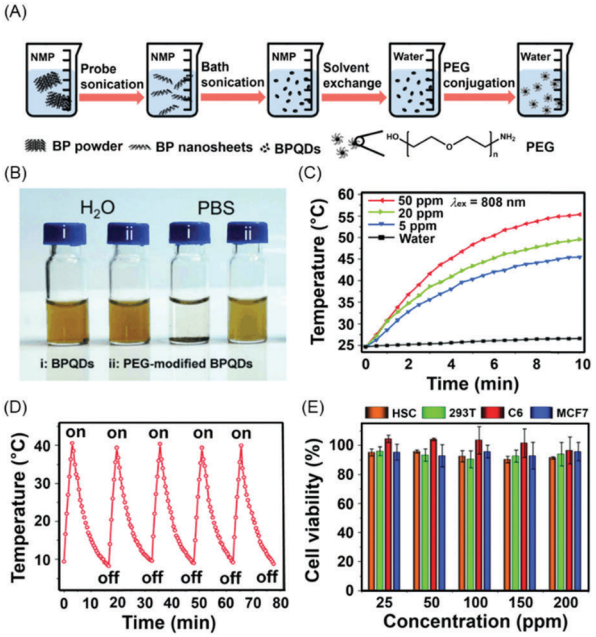

Fig. 9 (A) Synthesis and surface modification of BPQDs. (B) Photographs of BPQDs and PEG-modified BPQDs dispersed in water or PBS solutions. (C) Photothermal heating curves of pure water and PEGylated BPQD aqueous solutions under irradiation. (D) Heating of a suspension of PEGylated BPQDs in water for five laser on/off cycles. (E) Relative viabilities of HSC, 293T, C6 and MCF7 cells after incubation with various concentrations of PEG-modified BPQDs. Reproduced with permission from ref. 27, Copyright 2015, John Wiley and Sons.

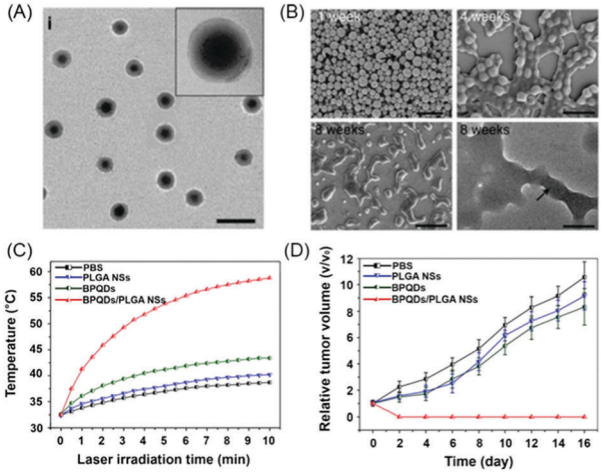

Fig. 10 (A) TEM image of BPQDs/PLGA nanospheres. (B) SEM images of BPQDs/PLGA nanospheres after degradation in PBS for 1, 4 and 8 weeks with the corresponding TEM image for 8 weeks. (C) Time-dependent temperature increase in MCF7 breast tumour-bearing nude mice under irradiation with different treatments. (D) Growth curves of the MCF7 breast tumour in nude mice with different treatments under NIR-laser irradiation. Reproduced with permission from ref. 22, Copyright 2016, Nature Publishing Group.

substantial potential of BPQDs as PTT agents in cancer treatment. Sun *et al.*[25] also applied a one-pot, solventless, high-energy mechanical milling technique to prepare water-soluble PEGylated FLBP with high biocompatibility. The resultant FLBP could efficiently convert NIR light into heat with excellent photostability. Sun *et al.* showed that an intratumour injection of PEGylated FLBP into mice bearing 4T1 tumour xenografts rapidly increased the temperature in the tumour region to 59 °C with low-power-density laser irradiation (2 W cm^{-2}) in 5 min, and the tumour could be totally removed by the therapy without any noticeable reoccurrence.

However, the biostability of FLBP in PTT strategies under physiological conditions remains unclear and is one of the most challenging tasks in BP projects. In this regard, in 2016, Shao *et al.*[22] reported biodegradable BPQDs/PLGA nanospheres prepared by encapsulation of BPQDs into PLGA, and the nanospheres showed a uniform spherical morphology with an approximately 100 nm size (Fig. 10A) and enhanced stability in a physiological medium for more than 4 weeks (Fig. 10B). The photothermal performance of BPQDs/PLGA nanospheres was significantly improved by the protection of the PLGA shell (Fig. 10C). Furthermore, the biodegradation behaviour of BPQDs/PLGA nanospheres was accelerated after the PLGA shell was first degraded. The biodegradation products were identified as phosphates and phosphonates. *In vitro* experiments showed that BPQDs/PLGA nanospheres show no significant cytotoxicity towards normal and tumour cells, even at a high concentration of BPQDs/PLGA nanospheres (100 ppm), and only 10 ppm of the BPQDs could efficiently kill almost all cancer cells when exposed to an NIR laser. Under NIR-laser irradiation, BPQDs/PLGA nanospheres triggered cancer cell apoptosis with a high tumour ablation rate in deep tumour tissues. Intratumoral administration of BPQDs/PLGA nanospheres into mice bearing 4T1 tumour xenografts rapidly increased the tumour temperature to 58.8 °C within 10 min under NIR-laser irradiation, leading to efficient and quick tumour ablation (Fig. 10D).

However, the hyperthermia triggered by PTT can potentially cause inflammatory disease, damage other nearby organs, and even lead to metastasis by inducing an undesirable heat shock response from a deep-seated tumour. To overcome this problem, advanced phototherapeutic strategies that can minimize side effects are strongly required.

3.2.2. Photodynamic therapy. Photodynamic therapy (PDT) was clinically approved for the treatment of several types of solid cancers as a minimally invasive emerging platform with specific spatiotemporal selectivity. In contrast to PTT, PDT relies on singlet oxygen ($^1O_2$) generated *via* energy transfer from a PS under suitable light irradiation to kill cancer cells. Many PSs such as noble metals, heavy atom-containing compounds, and organic molecules can efficiently generate $^1O_2$ from tissue oxygen under light irradiation, and they have shown a high capacity to selectively damage cancer cells owing to their preferable tumour accumulation and efficient intracellular translocation. However, PS applications are often limited by their poor water solubility, low quantum yield, and easy photobleaching. Therefore, new metal-free PSs with broad light absorption, high singlet oxygen quantum yields and excellent biocompatibility are in high demand.

In 2015, Wang *et al.*[15] first verified that exfoliated FLBP can be used as a PDT agent to efficiently generate $^1O_2$ under the entire

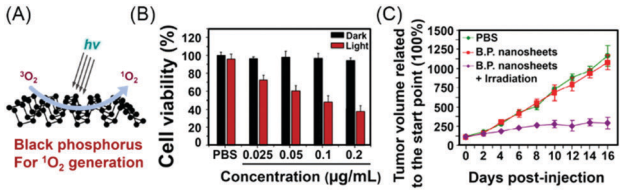

Fig. 11 (A) Schematic illustration of ROS generated by FLBP under irradiation. (B) Cell viability with different concentrations of FLBP. (C) Time-dependent tumour growth in a murine tumour model after treatments with different formulations. Reproduced with permission from ref. 15, Copyright 2015, American Chemical Society.

visible-light region with a quantum yield of 0.91 (Fig. 11A). The *in vitro* and *in vivo* experimental results indicated that water-dispersible FLBP shows a prominent PDT ability and photodegradable character as a cancer treatment agent (Fig. 11B and C). In this PDT technique, however, the penetration depth upon irradiation with conventional UV/visible light was controversial. Therefore, an NIR-responsive PDT PS was required to ensure that the PDT strategy was optimized for *in vivo* therapy. In 2016, Lv *et al.*[11] developed a new multifunctional nanocomposite based on FLBP for NIR-light-mediated PDT. Integration of poly(acrylic acid)-modified upconversion NPs (UCNPs) with FLBP resulted in UCNPs–FLBP composites *via* electrostatic interactions. Under NIR-light irradiation, the composite exhibited a good antitumour efficacy by generating ROS. At the same pump power, irradiation at 808 nm induced the strongest therapeutic effect compared with those observed with 650 and 980 nm. However, the low quantum yield in the upconversion process limited the clinical applications of this technique. To solve this problem, Yang *et al.*[7] developed a novel nanocomposite by assembling iron oxide (Fe_3O_4) NPs and AuNPs on FLBP (BP@Au@Fe_3O_4), and the nanocomposite has a broad light-absorption band and good photodegradation characteristics. *In vitro* and *in vivo* assays indicated that BP@Au@Fe_3O_4 NPs are highly biocompatible and exhibit an excellent tumour inhibition efficacy owing to the synergistic PTT and PDT mediated using a low-power NIR laser. BP@Au@Fe_3O_4 can anticipatorily suppress tumour growth by visualized synergistic therapy with magnetic resonance imaging (MRI).

3.3. Therapeutic agent delivery

In recent years, various drug delivery systems (DDSs) have been developed to administer pharmaceutical compounds and achieve an enhanced therapeutic effect in humans or animals. With the emergence and rapid development of multidisciplinary nanotechnology, desirable drug delivery strategies have been altered, and even more changes are anticipated in the near future. Over the past three decades, various 2D nanomaterials with tunable compositions, functional nanostructures, and unique morphologies have been investigated as platforms for therapeutic agent delivery, especially for cancer treatment. Among them, FLBP has a high surface area to volume ratio due to its puckered structure, which can enhance the drug-loading capacity of FLBP.

3.3.1. Chemotherapeutic agents. Chemotherapy is the simplest, cheapest, and most widely applied clinical treatment for cancer. However, non-target distribution of drugs may cause harmful side effects to healthy organs and tissues, inducing unwanted damage or pain, which limits further applications. A well-designed DDS can significantly reduce the side effects and improve the efficiency of traditional chemotherapeutic agents by concentrating the drug location and controlling the drug release and activation rates.

In 2016, Tao *et al.*[9] designed and prepared a FLBP-based robust DDS by liquid-phase exfoliation of bulk BP and efficiently loaded doxorubicin (DOX) onto the surface of FLBP (Fig. 12A). PEGylation significantly enhanced the drug-loading capability of BP-PEG NSs (up to 108%) compared with that of NP-based DDSs (usually 10–30%). Through colocalization experiments, the pathways of BP-PEG NS endocytosis into tumour cells were proven to be macropinocytosis and caveolae-dependent pathways. Furthermore, the BP-PEG NS function can be readily altered and fortified by changing its cargo and surface modification. For example, loading Cy7 dye results in BP-PEG/Cy7 NSs, which can be used as a good bioimaging system, and the folate targeting

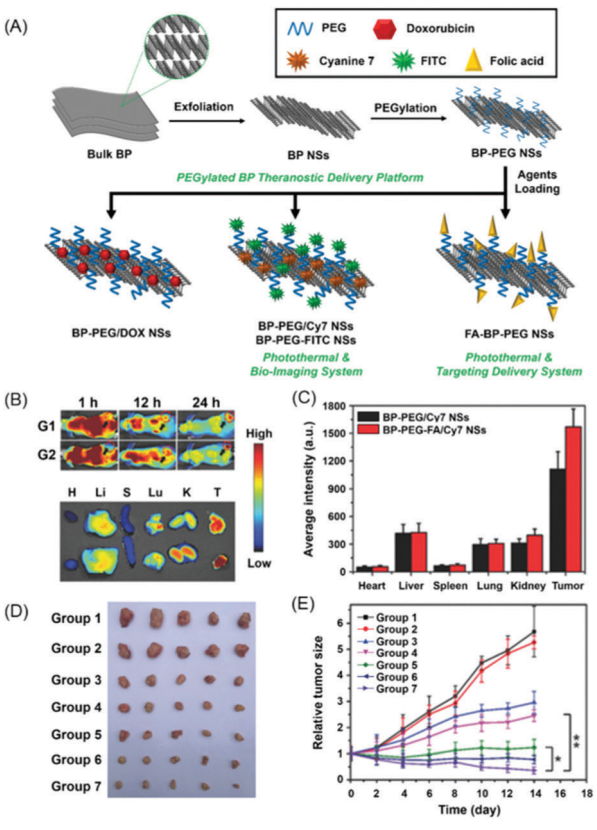

Fig. 12 (A) Schematic representation of the PEGylated FLBP theranostic delivery platform. (B) Time-lapsed NIR bioimaging of nude mice and NIR bioimaging of major organs and tumours after *in vivo* injection at 24 h. (C) Biodistribution of BP-PEG/Cy7 NSs and BP-PEG-FA/Cy7 NSs in nude mice measured by the average fluorescence intensities of the organs and tumours. (D) Morphologies of tumours removed from sacrificed mice. (E) Inhibition of HeLa tumour growth after different treatments (*$P < 0.05$, **$P < 0.01$). Group 1: saline; group 2: chloroquine (CQ); group 3: DOX; group 4: BP-PEG-FA/DOX; group 5: BP-PEG-FA + NIR; group 6: BP-PEG-FA + NIR + CQ; and group 7: BP-PEG-FA/DOX + NIR + CQ. Reproduced with permission from ref. 9, Copyright 2016, John Wiley and Sons.

moiety in BP-PEG-FA/DOX NSs is suitable for site-specific therapeutic applications. Moreover, due to the nature of FLBP materials, the cargo release rate of BP-PEG NSs can be quickly accelerated by NIR laser-induced hyperthermia as well as the acidic microenvironment of cancer regions (Fig. 12A). The *in vitro* therapeutic effects of BP-PEG NSs were evaluated with HeLa cells. The results of MTT assays indicated that BP-PEG-FA/DOX NSs can efficiently kill cancer cells even at a low DOX concentration (5 μg mL^{-1}) under 808 nm light irradiation for 10 min. In both *in vivo* and *ex vivo* imaging experiments, the BP-PEG-FA/DOX NSs provided a remarkable cancer recognition capability. Intravenous injection of BP-PEG-FA/DOX NSs boosted tumour accumulation by a receptor-mediated uptake of BP-PEG-FA/DOX NSs after 24 h incubation, compared with that observed with BP-PEG/DOX NSs (Fig. 12B and C). After repeating the injection and irradiation every 2 days for 2 weeks, the tumour volumes were significantly reduced (Fig. 12D and E) with minimal side effects, *i.e.*, the body weights of the mice remained almost unaffected. In summary, PEGylated FLBP is a promising delivery platform for cancer theranostics with excellent biocompatibility, low cytotoxicity, controlled release, and flexible modification.

Chen *et al.*[24] also applied FLBP as a platform for DOX drug delivery (Fig. 13A) and showed the high DOX loading capacity of FLBP (950%) due to its large surface area and electrostatic interactions. The DOX release rate of FLBP-DOX was 6-fold higher at pH 5.0 than that at pH 7.4 upon 808 nm laser irradiation, inducing effective, synergistic hyperthermia. In both *in vitro* and *in vivo* experiments, FLBP-DOX showed a good therapeutic effect for killing cancer cells, and the cellular uptake process was proven to be micropinocytosis (Fig. 13B and C). During the treatment, FLBP-DOX had excellent photostability, biocompatibility, biosafety, and synergistic therapeutic efficiency for PTT and DOX delivery. This FLBP-based DDS allows new perspectives for the development of multifunctional, 2D nanomaterial platforms and has substantial potential for broad clinical applications.

Recently, Qiu *et al.*[50] also developed a new concept of a FLBP hydrogel-based smart DDS, namely BP@hydrogel, by applying external NIR light to control anticancer drug delivery in cancer tissues. The BP@hydrogel underwent a sol/gel phase transition after intratumour injection and localized in the cancer tissue as a drug depot. FLBP, as a PS, converts the light into heat that softens and melts the drug-loaded, hydrogel-based nanostructure (Fig. 14A). Interestingly, the drug release rates can be accurately controlled by the light intensity, exposure duration, FLBP concentration, and hydrogel composition (Fig. 14B and C). Preclinical cancer models demonstrated that the NIR-light-induced decomposition of a BP@hydrogel accurately releases the anticancer drugs into tumour tissues (Fig. 14D). Noticeably, light irradiation of a biodegradable DOX-embedded BP@hydrogel eradicated subcutaneous breast and melanoma cancer cells without causing any adverse effects (Fig. 14E). Although breast and melanoma models were used as examples, this novel therapeutic system is expected to be effective for the treatment of most cancer types and exhibit potential for clinical cancer treatment.

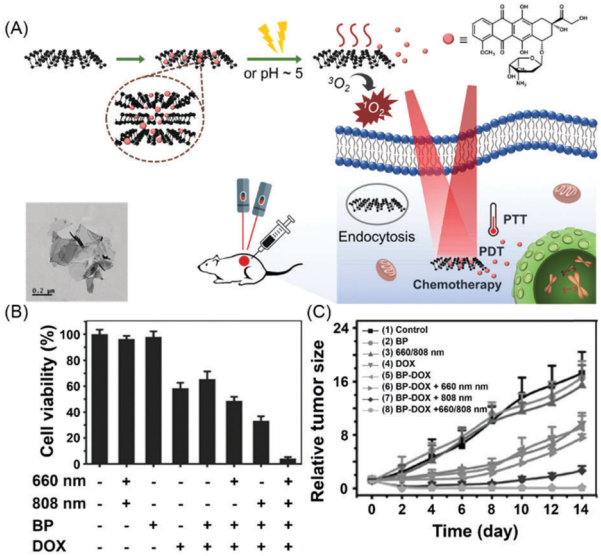

Fig. 13 (A) Schematic illustration of FLBP-based DDSs for the synergistic photodynamic/photothermal/chemotherapy of cancer and the TEM image of FLBP. (B) MTT assay of 4T1 cells under different treatments. (C) Tumour growth curves of tumour-bearing mice after different treatments. Reproduced with permission from ref. 24, Copyright 2016, John Wiley and Sons.

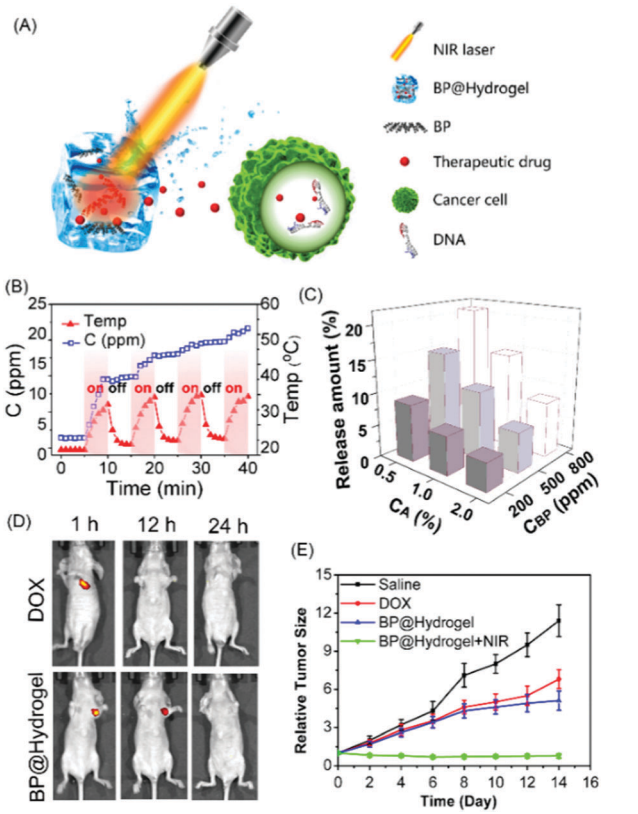

Fig. 14 (A) Schematic illustration of the BP@hydrogel working principle. (B) Photo-controlled temperature increase and release of DOX from the BP@hydrogel depot. (C) The release amount of DOX *vs.* the FLBP concentration and agarose content under irradiation. (D) FL images of mice 1, 12, and 24 h post-irradiation after the *in vivo* photothermal assay. (E) Tumour volumes of nude mice with breast tumours after various treatments. Reproduced with permission from ref. 50, Copyright 2017, National Academy of Science.

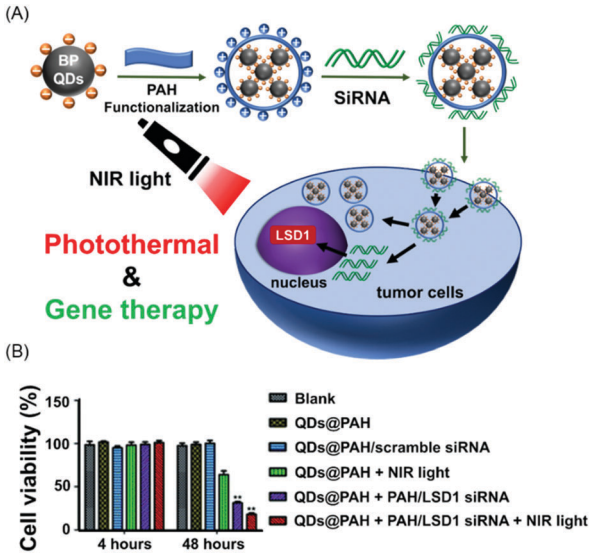

Fig. 15 (A) Schematic illustration of the BPQDs@PAH siRNA therapeutic mechanism. (B) Relative cell viabilities of PA-1 cells treated with different BPQD nanocomplexes without or with NIR light for 4 and 48 h. Reproduced with permission from ref. 12, Copyright 2017, Royal Society of Chemistry.

FLBP is also a useful delivery platform for other types of anticancer drugs in addition to DOX. Recently, Fojtu *et al.*[8] explored the applicability of FLBP loaded with two commercial platinum anticancer agents, cisplatin (CP) and oxaliplatin (OP). The binding abilities of cisplatin and oxaliplatin to the FLBP surface were examined by widescan X-ray photoelectron spectroscopy (XPS). The peaks from 72.5 to 76.5 eV confirmed the presence of Pt–P bonds in CP- and OP-bound FLBP. The binding between OP and FLBP was much stronger than that between CP and FLBP because of the presence of 1,2-diaminocyclohexane and an additional oxalate group in OP. Thus, FLBP–OP presented a higher cytotoxicity when assessed in the human ovarian cancer cell line A2780 after treatment for 24 h.

3.3.2. Gene therapy. Recently, FLBP has been applied for gene therapy. In 2017, Yin *et al.*[12] first applied BPQDs as gene delivery systems for further biomedical applications (Fig. 15A). Yin *et al.* reported PAH (polyelectrolyte polymer)-coated BPQDs can deliver lysine-specific demethylase 1 (LSD1) siRNA (small interfering RNA) into PA-1 cells (human ovarian teratocarcinoma), and the PAH modification enhanced the transfection efficiency of the BPQDs@PAH/siRNA nanocomplex (92.7%), which was much higher than those of lipofectamine 2000 and oligofectamine. Furthermore, a flow cytometry analysis indicated that LSD1 gene expression is inhibited and the mRNA level of SOX2, *i.e.*, the key substrate of LSD1, is down-regulated by BPQDs@PAH/siRNA. Importantly, the BPQDs@PAH/siRNA nanocomplex significantly inhibited PA-1 cell proliferation under NIR-light irradiation (Fig. 15B). Moreover, the combination of BPQDs@PAH/siRNA and PTT showed a higher cell killing capability than monotherapy.

3.4. Combination treatment

Due to the diversity of cancer types and the personal specificity of patients, monotherapy faces many problems such as drug resistance, serious side effects and long treatment cycles. In addition, anticipating the optimal efficacy and complete cure is difficult. In this regard, combination therapy is a new trend in cancer treatment and makes clinical applications more practical. However, developing a multifunctional system requires a complicated design and tedious synthesis procedure. Recently, therefore, advanced combination therapy using FLBP technology has attracted attention.

3.4.1. Theranostics. Theranostic agents are novel medicines that combine imaging and therapeutic functions, allowing simultaneous diagnosis, disease therapy, and treatment-response monitoring. FLBP is an ideal theranostic material that has intrinsic FL and PA properties for imaging as well as PTT and PDT properties for therapy. Moreover, FLBP can be easily reinforced and diversified by surface modification or cargo loading with very few synthetic steps, and diverse fluorophores can be linked to or loaded onto the surface of FLBP to perform *in vitro* or *in vivo* fluorescence imaging.[9] AuNPs can enhance the PTT efficacy of the whole system and endow the system with the potential to perform Raman biodetection with an improved SERS ability.[10] In addition, introducing iron oxide NPs and AuNPs onto FLBP can allow visualization of the therapy procedure with the aid of MRI.[7] Imaging data allow the bioactivities of FLBP-based nanosystems, such as transport pathways and cellular localization, to be understood, and the data contribute to pinpointing the tumour region for precise obliteration of malignant cells with reduced side effects. Therefore, diagnosis-guided therapy shows great potential in the biomedical field.

3.4.2. Synergistic therapy. As previously mentioned, FLBP has excellent photophysical properties that can generate $^1O_2$ under 660 nm laser irradiation for PDT and induce hyperthermia under 808 nm laser irradiation for PTT. In addition, FLBP material biodegradation can be accelerated by both hyperthermia and acidic environments. Because of these unique characteristics, FLBP-based nanocomposites can be easily modified for use in double- or triple-response therapy. When a drug is loaded onto the surface of FLBP *via* non-covalent interactions, a synergistic effect of chemotherapy, PDT and PTT with both 660 and 808 nm laser irradiation is observed.[24,51] This demonstrated that combination therapy is superior to monotherapy and can realize a highly synergistic performance and promote curative effects.

4. Conclusions and perspectives

This review comprehensively summarized recent progress in FLBP research on preparation methods, fundamental properties and biomedical applications. During the past three years, many studies have been conducted in the field of FLBP-based biomedicine. Compared with other prominent layered materials, such as graphene, TMDs and MXenes, phosphorene has many outstanding advantages for biomedical applications, including bioimaging, biosensing, phototherapy and drug delivery, due to its high mechanical strength, large surface area, desirable photoelectronic performance, high biosafety and excellent biocompatibility.

Table 1 Biomedical applications of FLBP and the corresponding modification strategies

Material	Preparation method	Morphology	Modification strategy	Characteristics	Bio-applications	Ref.
FLBP	Bath sonication in deionized water	4 nm thickness	PEI	Excellent biocompatibility; high stability under physiological conditions; broad light absorption band; photodegradable character under NIR light irradiation	MRI, PTT, PDT	7
FLBP	Bath and probe sonication in ice water	100 nm average size; 2–3 nm height	PEG-NH_2	High drug loading rate of 108%; the cargo release rate can be accelerated by both NIR and the acidic micro-environment of the cancer region	Drug delivery	9
FLBP	Probe and bath sonication in DMF	484 nm mean dimension	mPEG-SH	Enhanced SERS activity and PTT performance by Au	SERS imaging	10
FLBP	Bath sonication in NMP, HCl and deionized water	3 nm thickness	PEG-NH_2	NIR light excited PDT	PDT	11
FLBP	Bath sonication in distilled water	2.0 nm height	No	High quantum yield of singlet oxygen generation of 0.91	PDT	15
FLBP	Bath sonication in saturated NaOH solution of NMP	281 nm diameter; 5.5 nm thickness	No	DOX loading efficiency 950% in weight	PDT, PTT, drug delivery	24
BPNPs	Mechanical milling	3.2 nm diameter	PEG	PTCE 36.8%; excellent photostability and biocompatibility	PA imaging, PTT	25
BP nanodots	Bath sonication in distilled (deionized) water	10 nm diameter; 8.7 nm height	No	Excitation wavelength-dependent PL	PL imaging	26
BPQDs	Probe and bath sonication in NMP	2.6 nm diameter; 1.5 nm height	PEG-NH_2	Large extinction coefficient (14.8 L g^{-1} cm^{-1}); photothermal conversion efficiency (28.4%)	PTT	27
BPQDs	Probe and bath sonication in NMP	3.1 nm diameter of BPQDs; 102.8 nm diameter of BPQDs@PLGA nanospheres	PLGA	Biodegradable; high-efficiency photothermal performance	PTT	45
BPQDs	Bath sonication in NMP	2.8 nm diameter; 1.9 nm height	Sulfonic ester ligand of the titanium	Enhanced stability in water; excellent sensitivity and high spatial resolution in PA imaging	PA imaging	46

Although the vast biomedical application prospects of FLBP are very exciting and promising, biomedical exploration of FLBP is still relatively new compared to that of other 2D counterparts. Many critical issues still need to be systematically investigated. First, FLBP applications in various research fields are limited by its easy aggregation and fast degradation upon exposure to ambient conditions, which must be addressed for further biological applications. In this regard, many research groups still devote considerable efforts towards improving the dispersity and stability of FLBP in biological environments. However, the insufficient stability of FLBP is also regarded as biodegradability, which is desirable from the perspective of *in vivo* applications. The competition between FLBP instability and biodegradability should be considered by researchers designing and fabricating FLBP nanomaterials. Here, several reported strategies for FLBP modification and biomedical applications are summarized in Table 1. Second, as a novel, emerging nanomaterial, FLBP currently lacks biosafety and biocompatibility information. Thus, further systematic assessments should be performed for pervasive applications.

Furthermore, FLBP is an omnipotent platform for multidisciplinary biomedical applications because of its intrinsically superior properties. The synergistic effects of FLBP-based nanosystems have been demonstrated in some cancer treatment studies. More traditional or emerging methods, such as chemotherapy, gene therapy, and immunotherapy, can be combined with FLBP technology to enhance and broaden anticancer therapeutic action. In addition, FLBP-based treatments and FLBP technology should not be confined to only cancer-related fields, and several refractory diseases should be added to the list of potential applications. For example, the blood–brain barrier (BBB) is the main obstacle preventing researchers from curing neurodegenerative disorders (NDs), including Alzheimer's disease and Parkinson's disease. A recent study indicated that thermal effects can help particles penetrate the BBB and reach the brain. The discovery of FLBP, as a great PDT agent and nanocarrier, is a new direction for the design of new functional nanomaterials for the treatment of NDs and other cerebral diseases.

FLBP, a rising star of post-graphene 2D nanomaterial, is still in its infancy for biomedical applications. Extensive theoretical and experimental investigations are still underway to explore the potential of FLBP materials. Although particle size and surface modifications play critical roles in regulating the biological behaviours of FLBP, their relationships with other factors, such as transport pathways, systematic cytotoxicity and biological immunity, have yet to be deeply studied. Further and more in-depth exploitation of FLBP expertise and clinical transformation require contributions from chemical researchers, biomedical scientists, pharmacologists and industrial sectors. The continuous development of FLBP nanotechnology will provide limitless applications for various biochemical and medical areas, and more fundamental and technological breakthroughs are expected in the near future. We summarized and discussed recent FLBP-related studies to help researchers interested in designing new multifunctional FLBP-based nanosystems.

Abbreviations

2D	Two-dimensional
BP	Black phosphorus
FLBP	Few-layer black phosphorus
MXenes	Transition metal carbides, nitrides and carbonitrides
TMDs	Transition metal dichalcogenides
FETs	Field effect transistors
QDs	Quantum dots
NSs	Nanosheets
NPs	Nanoparticles
FL	Fluorescence
PA	Photoacoustic
SERS	Surface-enhanced Raman scattering
NIR	Near-infrared
PTCE	Photothermal conversion efficiency
PTT	Photothermal therapy
PDT	Photodynamic therapy
PS	Photosensitizer
ROS	Reactive oxygen species
EPR	Enhanced permeability and retention
DDSs	Drug delivery systems

Conflicts of interest

There are no conflicts to declare.

Acknowledgements

This work was supported by the CRI project of Korea (no. 2009-0081566, J. S. K.), the Basic Science Research Program through the National Research Foundation of Korea (NRF) funded by the Ministry of Education (NRF-2013R1A1A2062997, W. X. R.), a research fellowship grant from Korea University (W. X. R.), the National Natural Science Fund (China) (Grant No. 61435010 and 61575089, H. Z.), the Science and Technology Innovation Commission of Shenzhen (KQTD2015032416270385 and JCYJ20150625103619275, H. Z.), and the China Postdoctoral Science Foundation (2017 M610540, M. Q.).

Notes and references

1 K. S. Novoselov, A. K. Geim, S. V. Morozov, D. Jiang, Y. Zhang, S. V. Dubonos, I. V. Grigorieva and A. A. Firsov, *Science*, 2004, **306**, 666.
2 K. S. Novoselov, V. I. Fal'ko, L. Colombo, P. R. Gellert, M. G. Schwab and K. Kim, *Nature*, 2012, **490**, 192.
3 A. Castellanos-Gomez, L. Vicarelli, E. Prada, J. O. Island, K. L. Narasimha-Acharya, S. I. Blanter, D. J. Groenendijk, M. Buscema, G. A. Steele, J. V. Alvarez, H. W. Zandbergen, J. J. Palacios and H. S. J. van der Zant, *2D Mater.*, 2014, **1**, 025001.
4 S. Zhang, J. Yang, R. Xu, F. Wang, W. Li, M. Ghufran, Y. W. Zhang, Z. Yu, G. Zhang, Q. Qin and Y. Lu, *ACS Nano*, 2014, **8**, 9590.

5 F. N. Xia, H. Wang, D. Xiao, M. Dubey and A. Ramasubramaniam, *Nat. Photonics*, 2014, **8**, 899.
6 X. Ling, H. Wang, S. Huang, F. Xia and M. S. Dresselhaus, *Proc. Natl. Acad. Sci. U. S. A.*, 2015, **112**, 4523.
7 D. Yang, G. X. Yang, P. P. Yang, R. C. Lv, S. L. Gai, C. X. Li, F. He and J. Lin, *Adv. Funct. Mater.*, 2017, **27**, 1700371.
8 M. Fojtu, X. Y. Chia, Z. Sofer, M. Masarik and M. Pumera, *Adv. Funct. Mater.*, 2017, **27**, 1701955.
9 W. Tao, X. B. Zhu, X. H. Yu, X. W. Zeng, Q. L. Xiao, X. D. Zhang, X. Y. Ji, X. S. Wang, J. J. Shi, H. Zhang and L. Mei, *Adv. Mater.*, 2017, **29**, 1603276.
10 G. Yang, Z. Liu, Y. Li, Y. Hou, X. Fei, C. Su, S. Wang, Z. Zhuang and Z. Guo, *Biomater. Sci.*, 2017, **5**, 2048.
11 R. C. Lv, D. Yang, P. P. Yang, J. T. Xu, F. He, S. L. Gai, C. X. Li, Y. L. Dai, G. X. Yang and J. Lin, *Chem. Mater.*, 2016, **28**, 4724.
12 F. Yin, K. Hu, S. Chen, D. Y. Wang, J. N. Zhang, M. S. Xie, D. Yang, M. Qiu, H. Zhang and Z. G. Li, *J. Mater. Chem. B*, 2017, **5**, 5433.
13 C. C. Mayorga-Martinez, N. Mohamad Latiff, A. Y. Eng, Z. Sofer and M. Pumera, *Anal. Chem.*, 2016, **88**, 10074.
14 J. Peng, Y. Lai, Y. Chen, J. Xu, L. Sun and J. Weng, *Small*, 2017, **13**, 1603589.
15 H. Wang, X. Yang, W. Shao, S. Chen, J. Xie, X. Zhang, J. Wang and Y. Xie, *J. Am. Chem. Soc.*, 2015, **137**, 11376.
16 J. R. Brent, N. Savjani, E. A. Lewis, S. J. Haigh, D. J. Lewis and P. O'Brien, *Chem. Commun.*, 2014, **50**, 13338.
17 P. Yasaei, B. Kumar, T. Foroozan, C. Wang, M. Asadi, D. Tuschel, J. E. Indacochea, R. F. Klie and A. Salehi-Khojin, *Adv. Mater.*, 2015, **27**, 1887.
18 A. H. Woomer, T. W. Farnsworth, J. Hu, R. A. Wells, C. L. Donley and S. C. Warren, *ACS Nano*, 2015, **9**, 8869.
19 L. Z. Kou, C. F. Chen and S. C. Smith, *J. Phys. Chem. Lett.*, 2015, **6**, 2794–2805.
20 H. Liu, Y. Du, Y. Deng and P. D. Ye, *Chem. Soc. Rev.*, 2015, **44**, 2732.
21 M. Batmunkh, M. Bat-Erdene and J. G. Shapter, *Adv. Mater.*, 2016, **28**, 8586.
22 J. Shao, H. Xie, H. Huang, Z. Li, Z. Sun, Y. Xu, Q. Xiao, X. F. Yu, Y. Zhao, H. Zhang, H. Wang and P. K. Chu, *Nat. Commun.*, 2016, **7**, 12967.
23 Z. Sun, Y. Zhao, Z. Li, H. Cui, Y. Zhou, W. Li, W. Tao, H. Zhang, H. Wang, P. K. Chu and X. F. Yu, *Small*, 2017, **13**, 1602896.
24 W. Chen, J. Ouyang, H. Liu, M. Chen, K. Zeng, J. Sheng, Z. Liu, Y. Han, L. Wang, J. Li, L. Deng, Y. N. Liu and S. Guo, *Adv. Mater.*, 2017, **29**, 1603864.
25 C. Sun, L. Wen, J. Zeng, Y. Wang, Q. Sun, L. Deng, C. Zhao and Z. Li, *Biomaterials*, 2016, **91**, 81.
26 H. U. Lee, S. Y. Park, S. C. Lee, S. Choi, S. Seo, H. Kim, J. Won, K. Choi, K. S. Kang, H. G. Park, H. S. Kim, H. R. An, K. H. Jeong, Y. C. Lee and J. Lee, *Small*, 2016, **12**, 214.
27 Z. B. Sun, H. H. Xie, S. Y. Tang, X. F. Yu, Z. N. Guo, J. D. Shao, H. Zhang, H. Huang, H. Y. Wang and P. K. Chu, *Angew. Chem., Int. Ed.*, 2015, **54**, 11526.
28 P. W. Bridgman, *J. Am. Chem. Soc.*, 1914, **36**, 1344.
29 R. Hultgren, N. S. Gingrich and B. E. Warren, *J. Chem. Phys.*, 1935, **3**, 351.
30 S. Lange, P. Schmidt and T. Nilges, *Inorg. Chem.*, 2007, **46**, 4028.
31 L. Li, Y. Yu, G. J. Ye, Q. Ge, X. Ou, H. Wu, D. Feng, X. H. Chen and Y. Zhang, *Nat. Nanotechnol.*, 2014, **9**, 372.
32 A. Allain, J. Kang, K. Banerjee and A. Kis, *Nat. Mater.*, 2015, **14**, 1195.
33 W. Zhao, Z. Xue, J. Wang, J. Jiang, X. Zhao and T. Mu, *ACS Appl. Mater. Interfaces*, 2015, **7**, 27608.
34 M. B. Erande, M. S. Pawar and D. J. Late, *ACS Appl. Mater. Interfaces*, 2016, **8**, 11548.
35 C. Zhu, F. Xu, L. Zhang, M. Li, J. Chen, S. Xu, G. Huang, W. Chen and L. Sun, *Chemistry*, 2016, **22**, 7357.
36 J. Kang, S. A. Wells, J. D. Wood, J. H. Lee, X. Liu, C. R. Ryder, J. Zhu, J. R. Guest, C. A. Husko and M. C. Hersam, *Proc. Natl. Acad. Sci. U. S. A.*, 2016, **113**, 11688.
37 J. B. Smith, D. Hagaman and H. F. Ji, *Nanotechnology*, 2016, **27**, 215602.
38 Y. Xu, J. Yuan, L. Fei, X. Wang, Q. Bao, Y. Wang, K. Zhang and Y. Zhang, *Small*, 2016, **12**, 5000.
39 Y. Y. Zhang, X. H. Rui, Y. X. Tang, Y. Q. Liu, J. Q. Wei, S. Chen, W. R. Leow, W. L. Li, Y. J. Liu, J. Y. Deng, B. Ma, Q. Y. Yan and X. D. Chen, *Adv. Energy Mater.*, 2016, **6**, 1502409.
40 Y. Zhao, H. Wang, H. Huang, Q. Xiao, Y. Xu, Z. Guo, H. Xie, J. Shao, Z. Sun, W. Han, X. F. Yu, P. Li and P. K. Chu, *Angew. Chem., Int. Ed.*, 2016, **55**, 5003.
41 G. Qu, W. Liu, Y. Zhao, J. Gao, T. Xia, J. Shi, L. Hu, W. Zhou, J. Gao, H. Wang, Q. Luo, Q. Zhou, S. Liu, X. F. Yu and G. Jiang, *Angew. Chem., Int. Ed.*, 2017, **56**, 14488.
42 C. R. Ryder, J. D. Wood, S. A. Wells, Y. Yang, D. Jariwala, T. J. Marks, G. C. Schatz and M. C. Hersam, *Nat. Chem.*, 2016, **8**, 597.
43 J. D. Wood, S. A. Wells, D. Jariwala, K. S. Chen, E. Cho, V. K. Sangwan, X. Liu, L. J. Lauhon, T. J. Marks and M. C. Hersam, *Nano Lett.*, 2014, **14**, 6964.
44 Q. Zhou, Q. Chen, Y. Tong and J. Wang, *Angew. Chem., Int. Ed.*, 2016, **55**, 11437.
45 Z. N. Guo, H. Zhang, S. B. Lu, Z. T. Wang, S. Y. Tang, J. D. Shao, Z. B. Sun, H. H. Xie, H. Y. Wang, X. F. Yu and P. K. Chu, *Adv. Funct. Mater.*, 2015, **25**, 6996.
46 S. Yan, B. Wang, Z. Wang, D. Hu, X. Xu, J. Wang and Y. Shi, *Biosens. Bioelectron.*, 2016, **80**, 34.
47 V. Kumar, J. R. Brent, M. Shorie, H. Kaur, G. Chadha, A. G. Thomas, E. A. Lewis, A. P. Rooney, L. Nguyen, X. L. Zhong, M. G. Burke, S. J. Haigh, A. Walton, P. D. McNaughter, A. A. Tedstone, N. Savjani, C. A. Muryn, P. O'Brien, A. K. Ganguli, D. J. Lewis and P. Sabherwal, *ACS Appl. Mater. Interfaces*, 2016, **8**, 22860.
48 Y. T. Yew, Z. Sofer, C. C. Mayorga-Martinez and M. Pumer, *Mater. Chem. Front.*, 2017, **1**, 1130.
49 W. Gu, Y. H. Yan, X. Y. Pei, C. L. Zhang, C. P. Ding and Y. Z. Xian, *Sens. Actuators, B*, 2017, **250**, 601.
50 M. Qiu, D. Wang, W. Liang, L. Liu, Y. Zhang, X. Chen, K. David, C. Xing, Z. Li, B. Dong, X. Feng, D. Fan, S. Bao, H. Zhang and Y. Cao, *Proc. Natl. Acad. Sci. U. S. A.*, 2018, **115**, 501–506.
51 Y. Li, Z. Liu, Y. Hou, G. Yang, X. Fei, H. Zhao, Y. Guo, C. Su, Z. Wang and H. Zhou, *ACS Appl. Mater. Interfaces*, 2017, **9**, 25098.